

Na-montmorillonite hydrates under ethane rich reservoirs: $NP_{zz}T$ and $\mu P_{zz}T$ simulations

G. Odriozola,* J. F. Aguilar,† and J. López-Lemus‡
Programa de Ingeniería Molecular, Instituto Mexicano del Petróleo,
Lázaro Cárdenas 152, 07730 México, D. F., México

(Dated: May 7, 2021)

Na-montmorillonite hydrates in presence of ethane molecules are studied by means of hybrid Monte Carlo simulations in the $NP_{zz}T$ and $\mu P_{zz}T$ ensembles. The $NP_{zz}T$ ensemble allows us to study the interlaminar distance as a function of water and ethane content. These data show clear plateaus for lower ethane contents and mainly for water contents consistent with the formation of a single water layer. In addition, from this ensemble the structure for some of these interlaminar compositions were analyzed. For systems containing few ethane molecules and water enough to complete a single layer, it was observed that ethane mainly situates close to the interlayer midplane and adopts a nearly parallel arrangement to the clay surface. On the other hand, the $\mu P_{zz}T$ ensemble allows us to determine the interlaminar distance and water-ethane content for any specific reservoir. Here, some important findings are the following: the partial exchange of water by ethane molecules that enhances for decreasing the water vapor pressure; the obtention of a practically constant interlaminar space distance as a function of the water vapor pressure; the conservation of ion solvation shells; the enhancement of the water-ethane exchange for burial conditions; and finally, the incapability for a dehydrated clay mineral to swell in a dry and rich ethane atmosphere.

PACS numbers:

I. INTRODUCTION

Beyond the role that clay minerals play in several environmental and industrial processes, one major concern is how their presence affect petroleum migration and oil-recovery [1, 2]. In these processes, petroleum, natural gas, and their associated brines interact with clay minerals leading to retention, release, and selective adsorption of water, ions, and certain organic species, affecting the formation permeability. In general, the amount and kind of the adsorbed species depend on their chemical potential, which in turn establishes the swelling of a specific clay, for a given pressure and temperature. Hence, changes in the local reservoir composition or conditions, due to, for example, an oil-recovery process, can cause a destabilization of the formation clay minerals. This destabilization, together with a high percentage of clay mineral in the basin, may lead to a formation damage, *i. e.* diminution of the permeability. Therefore, knowledge of the clay behavior in presence of petroleum and natural gas compounds and its associated brines at reservoir conditions is mandatory for a better understanding of such processes.

One possible way to study these systems is by means of computer simulations. In the last few years, this tool has been widely used for studying the swelling of montmorillonite hydrates for different interlayer cations [3, 4, 5, 6, 7, 8, 9, 10, 11, 12]. There are, however, few theoretical works devoted to study the montmoril-

lonite behavior under basin conditions [13, 14, 15], and there are also few theoretical papers dealing with the interaction of montmorillonite hydrates with petroleum species [16, 17, 18, 19]. Hence, questions such as do any oil or natural gas compounds enter into the interlaminar space at reservoir conditions?, how many and what kind of molecules enter?, do they expel water molecules in the process?, and how does this affect the interlaminar space?, still do not have clear answers.

For tackling some of these questions we performed hybrid Monte Carlo (HMC) simulations to study the behavior of Na-montmorillonite hydrates at equilibrium with different ethane-water reservoirs. Ethane was chosen simply because it is an abundant natural gas and live-oil compound, and it is expected to enter into the interlaminar space. In addition, the Na^+ ion was chosen since it is the most abundant cation found in cation-clay-water systems. Simulations were carried out in the $NP_{zz}T$ and $\mu P_{zz}T$ ensembles. This last one has the advantage of allowing a direct measurement of the amount of molecules and the interlaminar distance at equilibrium under the established conditions. The employed water model is based on the TIP4P-water [20] and the Na^+ -water-clay interactions are given by Boek *et al.* [21]. The ethane parameters were taken from Nath *et al.* [22]. Two condition sets were studied. These are ground level, $P=1$ atm and $T=298\text{K}$, and $P=600$ atm and $T=394\text{K}$, which corresponds to a burial depth of 4 km (assuming average gradients of 30 K/km and 150 atm/km).

The paper is organized as follows. In Sec. II, we briefly describe the models and the methodology employed for performing the simulations. The results are shown in Sec. III. Finally, Sec. IV summarizes the main results and extracts some conclusions.

*godriozo@imp.mx

†aguilarf@imp.mx

‡jlemus@imp.mx

II. METHODOLOGY

A. The model

The Wyoming type montmorillonite cell given by Skipper *et al.* [23] was replicated in such a way to form a 4×2 layer. This layer has lateral dimensions of $L_x = 21.12 \text{ \AA}$ and $L_y = 18.28 \text{ \AA}$, and thickness of 6.56 \AA . To obtain a typical Wyoming type montmorillonite, isomorphous substitutions of trivalent Al atoms of the octahedral sites by divalent Mg atoms, and tetravalent Si by trivalent Al atoms were made. In this way, Clay I of the work by Chávez-Páez *et al.* [24] was obtained, with unit cell formula $\text{Na}_{0.75}n\text{H}_2\text{O}(\text{Si}_{7.75}\text{Al}_{0.25})(\text{Al}_{3.5}\text{Mg}_{0.5})\text{O}_{20}(\text{OH})_4$. Two layers were considered in the simulation box to avoid system size effects [24]. The rigid TIP4P model was used for water molecules [20] and a flexible model was considered for ethane molecules, just as described in the work by Nath *et al.* [22]. For the initial configuration, water and ethane molecules were randomly placed in the interlaminar spaces, and sodium ions were distributed in the interlayer midplanes. Note that six sodium ions per interlaminar space are needed to keep the system electroneutral. Periodical boundary conditions were applied in the three space directions.

The site-site intermolecular interactions are given by a Coulombian contribution plus a Lennard-Jones potential,

$$U_{ij} = \sum_{a,b} \left[\frac{q_a q_b}{r_{ab}} + 4\epsilon_{ab} \left[\left(\frac{\sigma_{ab}}{r_{ab}} \right)^{12} - \left(\frac{\sigma_{ab}}{r_{ab}} \right)^6 \right] \right] \quad (1)$$

where subindices i and j are molecular indexes, and a and b run over all sites of each molecule. Here, q_a and q_b are the charges of the corresponding sites, ϵ_{ab} and σ_{ab} are site-to-site specific Lennard-Jones parameters, and r_{ab} is the inter-site distance. The Lennard-Jones parameters for single sites are given in Table I. The bond stretching potential for ethane molecules is $U(r) = K_r(r - b_{eq})^2/2$, with $K_r = 191.765 \text{ kcal}/(\text{mol \AA})$ and $b_{eq} = 1.54 \text{ \AA}$ [25]. The site to site Lennard-Jones parameters are given by the Lorentz-Berthelot rules

$$\sigma_{ab} = \frac{\sigma_a + \sigma_b}{2}, \quad (2)$$

$$\epsilon_{ab} = \sqrt{\epsilon_a \epsilon_b} \quad (3)$$

We should point out that the oxygen-oxygen parameters' values were chosen to be exactly those of the TIP4P water model. These values were slightly changed in references [14, 21, 24]. In addition, the sodium ion parameters were obtained by a fitting procedure that leads to a relatively good agreement between the pair energies obtained from equations (7) and (8) of Bounds's work [26] and equation (1). These are, in fact, also similar to those reported by Boek *et al.* [21]. The fitting procedure was performed by employing the Levenberg-Marquardt

TABLE I: Lennard-Jones parameters for ethane-water-clay- Na^+ interactions.

Sites	ϵ (kcal/mol)	σ (\AA)
O	0.155	3.154
H	0.000	0.000
Na	1.570	1.740
Si	3.153	1.840
Al	3.153	1.840
Mg	3.153	1.840
CH_3	0.1990	3.825

algorithm and considering several positions and orientations of the water-ion pair. To check the accuracy of the fitted expression, a HMC simulation of 216 water molecules and a Na^+ ion (and a Cl^- ion to keep the system electroneutral) was performed. The obtained Na^+ -oxygen and Na^+ -hydrogen radial distribution functions, $g(r)$, and coordination numbers, $n(r)$, were very similar to those reported by Bounds [26]. Finally, parameters for Si were taken from Marry *et al.* [27]. Parameters for Al and Mg were assumed to be equal to those of Si.

The Ewald summation formalism was implemented for handling the electrostatic interactions. For this purpose, we set the convergence factor to $5.6/L_{min}$, being L_{min} the minimum simulation box side. Five reciprocal lattice vectors for the directions along the shortest sides and six for the direction along the largest side were set [28]. For the Lennard-Jones contribution a spherical cutoff of $L_{min}/2$ was considered. In addition, this contribution was corrected by the standard methods for homogeneous fluids [29].

B. Simulations

A hybrid Monte Carlo scheme was employed for the simulations. This technique has the advantage of allowing global moves while keeping a high average acceptance probability. A global move in configuration space consists in assigning velocities and integrating the system over phase space using some discretization scheme [30]. Velocities are randomly assigned from a Gaussian distribution in correspondence with the imposed temperature and in such a way that total momentum equals zero for both interlaminar spaces. The discretization scheme we employed is a reversible multiple time scale algorithm based on the Trotter expansion of the Liouville propagator, which has the advantage of allowing to split forces into short and long range ones [31]. Hence, a short time step is employed to generate the motion using the rapid varying short range forces, and a long time step is used only to correct the velocities by using the slow varying long range forces. The short range forces were chosen as the Lennard-Jones contribution plus the real part of the electrostatic potential, and the long range forces were set

as the reciprocal space contribution of the electrostatic potential. This allows reducing the expensive calls to the reciprocal space contribution. For diminishing time correlations, a new configuration is obtained after ten integration steps. Once the new configuration is generated, it is accepted with a probability

$$P = \min\{1, \exp(-\beta\Delta\mathcal{H})\} \quad (4)$$

where $\Delta\mathcal{H}$ is the difference between the Hamiltonians associated to the new and previous configuration and β is the inverse of the thermal energy. Note that increasing the time step will result in a larger deviation from total energy conservation and so, in a lower average acceptance probability. We fixed the long time step to eight times the short time step, and we set the short time step to obtain an average acceptance probability of 0.7 [30]. For more details about the hybrid Monte Carlo algorithm see Mehlig *et al.* [30].

For sampling in the $NP_{zz}T$ ensemble, after a trial change of particles' positions, a box change is attempted in such a way that the stress normal to the surface of the clays, P_{zz} , is kept constant. For this purpose, box fluctuations are allowed only in the z -direction and the probability for accepting a new box configuration is given by

$$P = \min\{1, \exp[-\beta(\Delta\mathcal{U} + P_{zz}\Delta V - N\beta^{-1}\ln(V_n/V_o))]\} \quad (5)$$

Here, $\Delta\mathcal{U}$ is the change in the potential energy, ΔV is the volume change, N is the total number of molecules, and V_n and V_o are the new and old box volumes, respectively [24].

For sampling in an open ensemble, the possibility of insertions and deletions of water and ethane molecules has to be considered. Water insertions and deletions

were performed by Rosenbluth sampling as explained elsewhere [32]. The only difference is that we account for the real part of the electrostatic contribution for the hydrogen trial conformations (including the non massive TIP4P site contribution). This is a necessity since the TIP4P hydrogen sites do not have a dispersion-repulsion contribution, in contrast to the MCY water model they employed. Hence, the real part of the electrostatic contribution appears directly in the Rosenbluth factors and must not be included in the exponential part of equations (5) and (6) of the work by Hensen *et al.* [32]. Similarly, insertions and deletions of ethane molecules were also performed by the Rosenbluth method. Here, the slight difference is that ethane molecules are flexible. In this case, the method is clearly explained elsewhere [33].

Commonly, the open ensemble employed in simulations is the Grand canonical, *i. e.* the μVT ensemble. This was successfully employed to determine the stable hydration states of the water-ion-clay systems, *i. e.* the number of water molecules and the interlaminar space at equilibrium with a given reservoir [5, 14, 24, 32, 34]. For this purpose, it is necessary to measure the pressure as a function of the interlaminar distance (volume) to determine the states that produce the reservoir's pressure. The problem is that this implies a large number of simulation runs. Another possibility would be sampling in the $\mu P_{zz}T$ ensemble. In this way, a single simulation run is employed for obtaining the system at equilibrium with the reservoir's conditions.

For finding an algorithm capable for sampling such ensemble, it is necessary to pay attention on the probability density of finding the system in a particular configuration. This is deduced from the partition function, which in this case reads as

$$\mathcal{Q}_{\mu_1\mu_2P_{zz}T} \propto \sum_{N_1, N_2=0}^{\infty} \frac{\exp[\beta(\mu_1 N_1 + \mu_2 N_2)]}{\Lambda^{3N} N_1! N_2!} \int dV \exp[-\beta P_{zz} V] V^N \int d\mathbf{s}^N \exp[-\beta\mathcal{U}(\mathbf{s}^N)] \quad (6)$$

where Λ is the thermal de Broglie wavelength, subindexes 1 and 2 refer to components 1 and 2 (water and ethane), and \mathbf{s}^N are scaled coordinates [33]. Hence, the corresponding probability density of finding the system in a particular configuration is given by

$$\mathcal{N}_{\mu_1\mu_2P_{zz}T} \propto \frac{V^N \exp\{-\beta[\mathcal{U}(\mathbf{s}^N) - \mu_1 N_1 - \mu_2 N_2 + P_{zz} V]\}}{\Lambda^{3N} N_1! N_2!} \quad (7)$$

and so, the algorithm must sample this distribution. For this purpose, it is easy to show that particle movements, insertions and deletions, and box changes must be done as in typical NVT , μVT and $NP_{zz}T$ sampling [33]. In

particular, after trying a change of particles' positions, we perform several attempts of inserting-deleting water and ethane molecules. This is done by randomly calling the four possible trials in such a way that all calls are equally probable. This is important in order to guaranty the establishment of detail balance. Since accepting insertions or deletions are rare, we repeat this step 10 times or until accepting any insertion or deletion. In case of refusing the 10 insertion-deletion trials, we performed a box trial move. In this way, the system rapidly evolves to an equilibrium state that, in general, depends on the initial conditions.

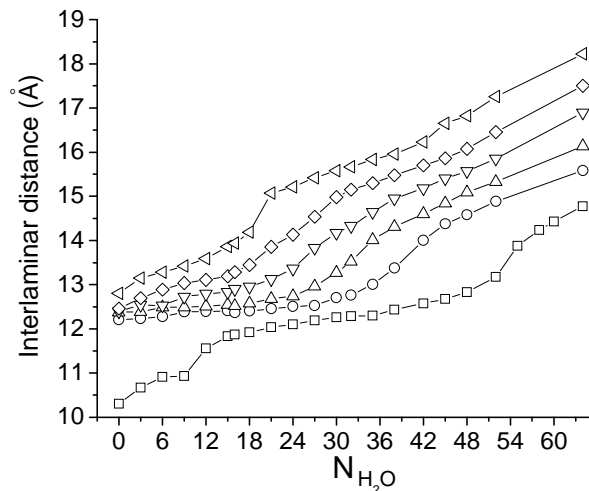


FIG. 1: Interlaminar distance as a function of the number of water molecules per interlamina space. Symbols \square , \circ , \triangle , ∇ , \diamond and \triangleleft correspond to 0, 6, 9, 12, 15 and 18 fixed ethane molecules, respectively.

III. RESULTS

In order to organize the results this section is split into two parts. These are *Sampling in the $NP_{zz}T$ ensemble* and *Sampling in the $\mu P_{zz}T$ ensemble*. Each part presents the results for the conditions of ground level and for 4 km of burial depth. These are $T=298$ K, $P=1$ atm and $T=394$ K, $P=600$ atm, respectively.

A. Sampling in the $NP_{zz}T$ ensemble

This ensemble allows measuring the interlaminar distance as a function of the imposed number of water and ethane molecules for a given temperature and pressure. This means that water and ethane content may or may not correspond to real systems.

Fig. 1 shows the interlaminar distance as a function of the number of water molecules per clay sheet. Here, the ethane content is fixed and the established conditions correspond to ground level. Naturally, it is observed that as far as the ethane content increases, the curves reach larger interlaminar distances. Hence, the bottom curve corresponds to zero ethane molecules and the uppermost curve to 18 ethane molecules per interlamina space. It should be pointed out that this lowest curve is in good agreement with others reported elsewhere [24], suggesting that the differences in models and methods are not very important. This curve starts from an interlaminar distance of 10.22 Å, where ions are the only specie. This dehydrated state is in good agreement with those reported for the TIP4P water model [21, 24, 34] and slightly larger than the reported experimental values (9.8 - 10.0 Å) [35]. The curve grows with increasing water con-

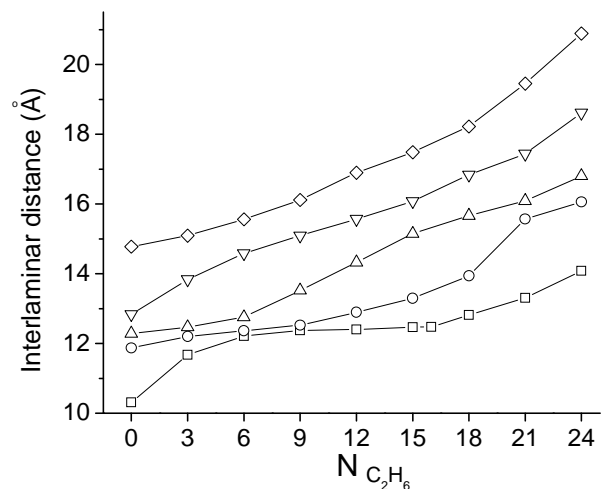


FIG. 2: Interlaminar distance as a function of the number of ethane molecules per interlamina space. Symbols \square , \circ , \triangle , ∇ and \diamond correspond to 0, 16, 32, 48 and 62 fixed water molecules, respectively.

tent reaching a plateau for 20-48 water molecules. This plateau yields interlaminar spaces in the range 12.0-12.7 Å, in good agreement with experimental data. For larger water contents, a second plateau is developed, which corresponds to a double water layer.

When six ethane molecules are added to the interlamina space, a large plateau is developed in the water content range of 0-27, which corresponds to interlaminar spaces ranging in 12.2-12.5 Å. This means that as early as few ethane molecules enter into the interlamina space, they force it to yield relatively large interlaminar distances and so, additional water molecules easily enter without changing it. Furthermore, the fact that only 27+6 total molecules saturate the first layer implies that ethane molecules occupy approximately the triple effective volume than water. This is verified by the fact that for 9 and 12 ethane molecules the plateaus shorten, disappearing for 15 ethane molecules per interlamina space. Note that in each case the plateaus are yielded for 0-18 and 0-6 water molecules, respectively. We should also pointed out that in all cases the plateaus produce interlaminar spaces in the range of 12.2-12.5 Å. Hence, if ethane goes into the interlamina space, it is expected to displace water in the process without affecting the interlaminar distance. In addition, these facts make us think that for a single layer and in the most favorable situation, 12 ethane molecules may enter into the interlamina space, displacing approximately 36 water molecules in the process.

Similar conclusions can be drawn by studying the interlaminar distance as a function of the number of ethane molecules keeping fixed the number of water molecules. This was done and it is presented in Fig. 2. As can be seen, the plateaus for 0, 16 and 32 water molecules correspond to the ranges 6-16, 3-9 and 0-3 ethane molecules,

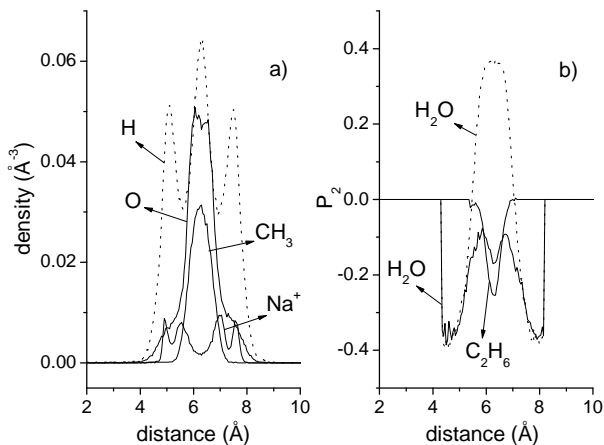


FIG. 3: a) Density profiles of oxygen, hydrogen, methyl, and sodium sites. They were obtained by fixing 27 water and 6 ethane molecules. b) The corresponding second Legendre polynomial order parameters for water and ethane (see text).

respectively. In addition, the corresponding interlamellar distances are in the range 12.2-12.5 Å. No other plateaus are seen for larger water contents. In summary, these results confirm the conclusions extracted from the preceding paragraph.

Let us focus on the structure of the particular configuration of 27 water and 6 ethane molecules per interlamellar space. This is shown in Fig. 3, where the density profiles of oxygen, hydrogen, methyl, and sodium sites are plotted vs. the interlamellar distance from the clay surface. Note that oxygen, hydrogen, and sodium profiles are nearly equal to those reported by Chávez-Páez *et al.* [24]. That is, we observed the same peaks at the same distances for the different species. The only difference is that the water peaks are shorter due to their smaller content. Hence, the presence of ethane molecules does not practically affect the structure of water and ion sites. In other words, ethane molecules do not seem to interact very much with water molecules and ions.

To study the orientation of ethane and water molecules as a function of the interlamellar position, we compute the statistical average of the second Legendre polynomial order parameter

$$P_2 = \langle 3 \cos^2(\theta_i)/2 - 1/2 \rangle \quad (8)$$

for all molecules, i . In case of water, the interlamellar oxygen position and two angles were considered. The first one formed between the dipole moment vector of the considered water molecule and a vector normal to the clay layers (reference vector). The other one is formed between the hydrogen-hydrogen direction and the reference vector. These are shown in Fig. 3 b) as solid and dashed lines, respectively. In case of ethane, the position of the center of mass of each molecule and the angle formed between the methyl-methyl direction and the reference vector were considered. Hence, a positive value of P_2 means a tendency for the vectors to get parallel to the

normal of the clay sheets, whereas a negative value of P_2 indicates a tendency for the vectors to get perpendicular to the reference vector.

It is observed at the interlayer midplane that the water molecules show a small tendency to have their dipole moment vectors normal to the reference vector. Furthermore, they also show a tendency to have their H-H-vectors parallel to the reference vector. For water molecules closer to the clay surfaces, however, the H-H-vectors turn perpendicular to the reference vector and their dipole vectors become more normal to the reference vector. These results are in good agreement with other works [3, 15]. There are, however, some differences of behavior between the TIP4P and the MCY-water molecules previously studied by us [15]. That is, for the TIP4P water we do not observe those few water molecules that escape from the midplane and stick to the siloxane surface that were observed for the MCY-water model. On the other hand, ethane molecules were observed to show a tendency to align parallel to the clay surfaces.

To study how the confinement and ethane presence affect the ions solvation, the radial distribution functions and coordination numbers for sodium-oxygen sites were built (not shown). Here, total oxygen sites were split in water and clay oxygen sites so that we can distinguish between the different contributions. It was observed that all $g(r)$ peak at 2.31 Å, leading to a total coordination number of 5.9 and a partial coordination number for the water molecules of 3.7. Hence, sodium ions lose on average more than two water molecules of their first shell to coordinate with clay oxygen sites. In addition, the total coordination number of 5.9 suggests that sodium ions are far from ethane molecules, indicating that ethane molecules are being left aside. We should also mention that since oxygen-oxygen separations on the clay surface are significantly smaller than oxygen-oxygen separations for waters of hydration shells around sodium ions, the total coordination numbers may be somewhat inflated. This may question the validity of some of these conclusions.

The radial distribution functions for the methyl-oxygen, -sodium, -hydrogen and -methyl sites were also obtained and are shown in Fig. 4. In case of oxygen sites, they were again split into the corresponding water and clay contributions. It is observed that all first methyl-oxygen peaks are situated at 3.55 Å as well as the methyl-hydrogen peak. Such structures are reminiscent of those observed in hydrophobicity investigations and are a result of water-water hydrogen bonding, since it is observed a lack of hydrogen atoms pointing toward the nonpolar solute. Note that the second methyl-oxygen peak appears at 4.97 Å, corresponding to the farthest methyl of the ethane molecule. This is also seen for the methyl-methyl distribution function, where a double peak at 4.13 Å and 5.13 Å is observed. It should be pointed out that the peak for the methyl-sodium distribution function appears as far as 5.67 Å. This means that, in general, the water coordination shell that surrounds ions prevents the

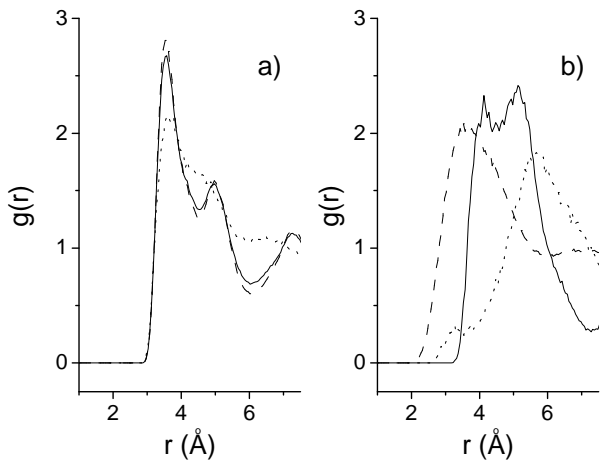


FIG. 4: a) Radial distribution functions for methyl-oxygen sites. Dotted, dashed and solid lines correspond to water, clay and total oxygen sites, respectively. b) Radial distribution function for methyl-sodium (dotted line), methyl-hydrogen (dashed line) and methyl-methyl (solid line) sites.

ethane molecules to approach them. Nevertheless, a very small shoulder appears at 3.25 Å, meaning that a few ion shells were partially broken or that the number of water molecules were not enough to complete them. This may explain the 5.9 coordination number of sodium ions by oxygen atoms, instead of the 6.0 value we found for bulk.

Fig. 5 depicts some observations mentioned above, where a snapshot of this system is presented. Here, a side view shows how water molecules coordinate with ions in the middle of the topmost layer displacing ethane molecules. The same topmost layer configuration is also seen as a top view, where the solvation of sodium ions and the isolation of the ethane molecules are more evident. This also happens in the lowest layer, although it is not clearly shown. Furthermore, it should be noted that ethane molecules are located practically in the middle of the interlamellar space where they are parallel to the clay surfaces, as previously mentioned.

Fig. 6 shows the density profiles of the interlamellar sites for the system containing 52 water and 6 ethane molecules. It is clearly seen that two well defined oxygen peaks indicate the formation of a double water layer. Hydrogen atoms show two peaks for each oxygen peak, a larger one close to the clay surface, and a smaller one almost overlapping its corresponding oxygen peak. Sodium ions show three peaks, a larger one at the interlayer mid-plane and two smaller ones close to the clay surfaces. These observations are practically equal to those found elsewhere [14]. Again, the only difference seems to be the height of the peaks, which is easily explained by the smaller water concentration in the interlayer.

The orientation of water molecules is similar to the one layer case. It is observed a dipole moment vector and a H-H-vector mostly parallel to the clay surface for those water molecules close to it. For the water molecules

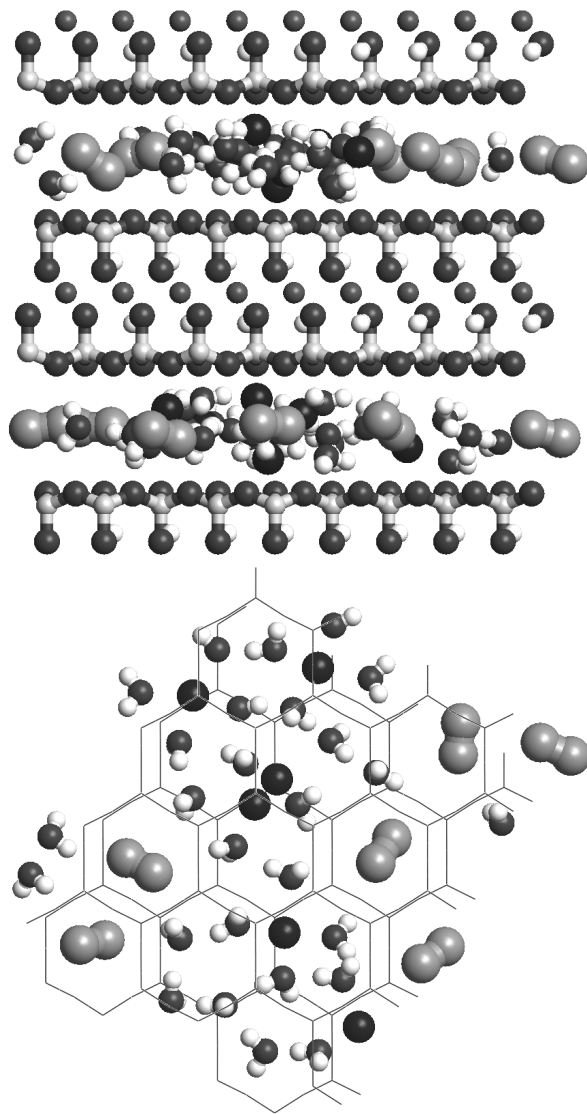


FIG. 5: Snapshot of an equilibrated system having 27 water molecules and 6 ethane molecules per interlamellar space. Here, H are white, CH₃ are light gray, O are dark gray and Na sites are black. Two views of the same configuration are shown, a side view at the top and a top view at the bottom. Note that for clarity, the bottom view shows only the topmost layer, representing the clay structure by lines.

placed over the oxygen peak, it is obtained a positive second Legendre order parameter for the H-H-vector and even a slightly positive one for the dipole moment vector. This means that both tend to align perpendicular to the clay surface. On the other hand, the ethane molecules behave quite differently than in the previous case. Here, although they still situate in the midplane of the interlamellar space, one CH₃ site situates closer to the upper clay surface and the other one situates closer to the lower. Hence, and as can be seen in Fig. 6 b), ethane molecules tend to align perpendicular to the clay surfaces. This

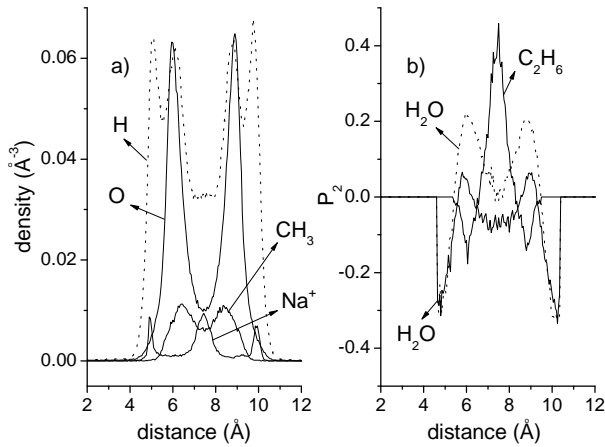


FIG. 6: a) Density profiles of oxygen, hydrogen, methyl, and sodium sites. They were obtained by fixing 52 water and 6 ethane molecules. b) The corresponding second Legendre polynomial order parameter for water and ethane.

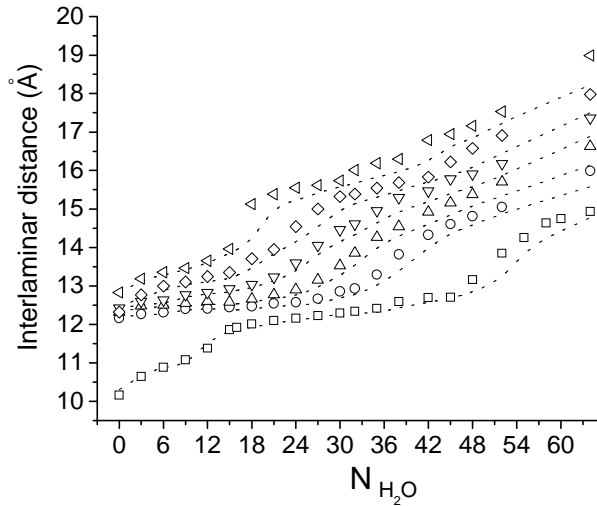


FIG. 7: Interlaminar distance as a function of the number of water molecules per interlaminar space. Symbols \square , \circ , \triangle , ∇ , \diamond and \triangleleft correspond to 0, 6, 9, 12, 15 and 18 fixed ethane molecules, respectively. The data is obtained for 4 km of burial depth. The corresponding data obtained for ground level conditions (Fig. 1) are presented as dotted lines.

explains the two CH_3 peaks shown in Fig. 6 a).

The interlaminar distance as a function of the number of water molecules for 4 km of burial depth is shown in Fig. 7. The different data series correspond, as in Fig. 1, to different ethane contents. This figure also shows as dotted lines the data obtained for ground level conditions. This is just to make easier the comparison. As can be seen, the same trend is observed for both conditions. The only difference is that for 4 km of burial depth the interlaminar distances are larger than for the ground level case. This difference is not very pronounced in any case, but seems to be larger for those systems contain-

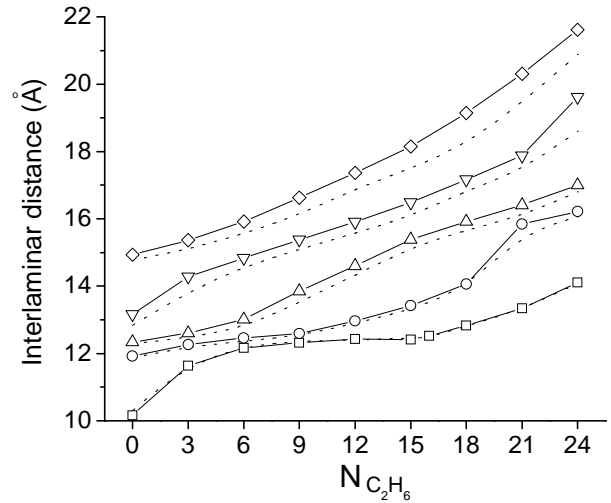


FIG. 8: Interlaminar distance as a function of the number of ethane molecules per interlaminar space. Symbols \square , \circ , \triangle , ∇ and \diamond correspond to 0, 16, 32, 48 and 62 fixed water molecules, respectively. The data is obtained for 4 km of burial depth. The corresponding data obtained for ground level conditions (Fig. 2) are presented as dotted lines.

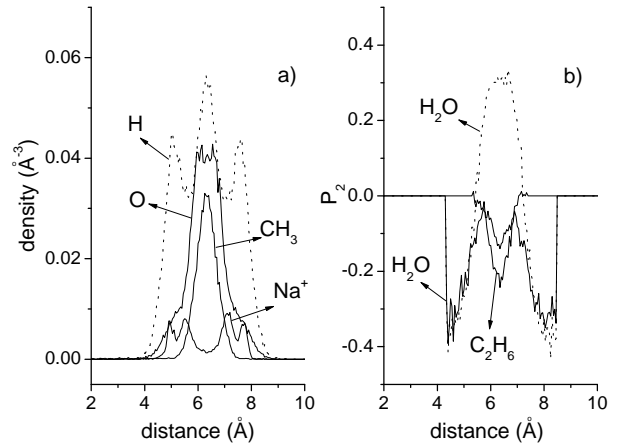


FIG. 9: a) Density profiles of oxygen, hydrogen, methyl, and sodium sites. They were obtained by fixing 27 water and 6 ethane molecules, and for 4 km of burial depth. b) The corresponding second Legendre polynomial order parameter for water and ethane.

ing a larger number of molecules. Similarly, Fig. 8 shows the interlaminar distance as a function of the number of ethane molecules, keeping the number of water molecules fixed. Furthermore, and as in the previous figure, the data obtained for ground level is presented as dotted lines. Again, it is observed that the tendencies are similar although larger interlaminar distances are obtained for the largest temperature and pressure case. These findings are similar to those previously reported by us [15].

Finally, the density profiles and second Legendre poly-

nomial order parameters for the different sites are shown in Fig. 9, for the system having 27 water and 6 ethane molecules and for 4 km of burial depth. As can be seen, both, density profiles and order parameters are very similar to those obtained for ground level conditions (see Fig. 3). Nevertheless, the peaks are wider and shorter than those obtained for ground level conditions, indicating a larger disorder of the interlayer structure. This is in good agreement with previous simulations [14, 15] and experiments [36].

B. Sampling in the $\mu P_{zz} T$ ensemble

As mentioned in section IIB, this ensemble allows obtaining the interlaminar distance, water content and ethane content for the studied system at equilibrium with any given reservoir's conditions. For that purpose, the chemical potential of the species contained in the reservoir at given conditions must be known. Hence, expression $\beta\mu = \beta\mu_0 + \ln(p/p_0)$ was used, where p_0 is the vapor pressure at equilibrium with liquid water whose chemical potential is μ_0 , and p is the vapor pressure. For the TIP4P water model and for $T=298$ K and $P=1$ atm, we obtained $\beta\mu_0 = -17.4$ by simulating 200 water molecules in a cubic box. This value is in good agreement with others reported for the same model [24]. For the studied burial conditions, *i. e.*, for $T=394$ K and $P=600$ atm, we obtain $\beta\mu_0 = -13.4$.

For obtaining the water chemical potential, we employed the Rosenbluth insertion method as described in detail elsewhere [32, 33]. For this purpose, $k_o=100$ oxygen trial sites are randomly chosen inside the simulation box and the quantity $\exp[-\beta u_i]$ is evaluated for each case. Here, u_i is the potential energy for a particular oxygen site that comes only from the Lennard-Jones contribution. Immediately after, a favorable oxygen site is selected by assigning to each site the probability $P_i = \exp[-\beta u_i]/W_o$ with $W_o = \sum_i \exp[-\beta u_i]$. For this selected oxygen site, $k_h=20$ hydrogen configurations are tried while the quantity $\exp[-\beta u_j]$ is calculated. In this case, u_j contains the contribution of the real part of the electrostatic potential. Hence, both hydrogen atoms and the charged non massive site of the TIP4P molecule contribute to u_j . Again, a favorable orientation is selected by assigning to each one the probability $P_j = \exp[-\beta u_j]/W_h$ where $W_h = \sum_j \exp[-\beta u_j]$. Once the TIP4P molecule is fully inserted, the reciprocal space contribution to the electrostatic potential, u_r , is evaluated. Finally, the Rosenbluth weight factor is $W_{H_2O} = W_o W_h \exp[-\beta u_r]/(k_o k_h)$. Since we perform the sampling from a $N P_{zz} T$ ensemble, the chemical potential finally reads [33]

$$\beta\mu = -\ln\left(\frac{1}{\beta P_{zz} \Lambda^3}\right) - \ln\left(\frac{\beta P_{zz}}{N+1} \langle V W_{H_2O} \rangle\right) \quad (9)$$

where $\langle \dots \rangle$ is the average obtained over 100000 configurations in which 10 water insertions per configuration

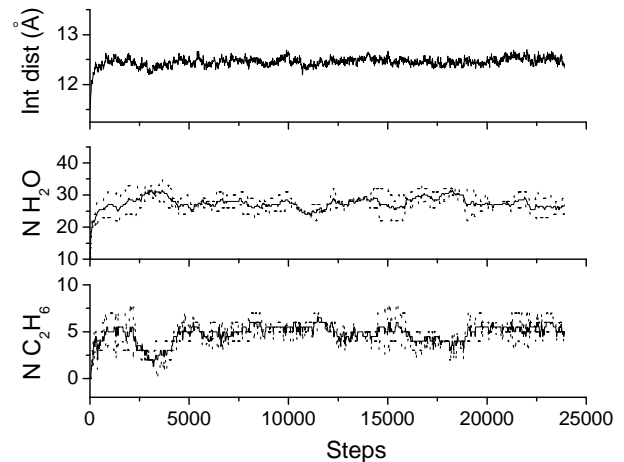


FIG. 10: Typical evolution of the interlaminar space, water, and ethane content. Solid lines are averages whereas dashed lines correspond to each interlaminar space. The established conditions were $T=298$ K, $P=1$ atm, $p/p_0=0.1$ and $p_e = 0.893P$. Initial conditions were established as 11.5 Å of interlaminar space and 10 water molecules.

were done.

On the other hand, we use the relationship $\beta\mu = \beta\mu_{id.gas}^0 + \ln(\beta p_e/\Phi)$ where $\mu_{id.gas}^0$ is the ideal gas chemical potential of the reference state, p_e is the ethane partial pressure, and Φ is the ethane fugacity coefficient [33]. This coefficient is 0.992 for ground level conditions (taken from Din [37]) and 0.536 for 4 km of burial depth (extrapolation of the data given by Din [37]).

In this way, for ground level conditions and for a reservoir having $p/p_0 = 0.1$ and $p_e = 0.893P$, Fig. 10 shows how the system reaches equilibrium starting from a configuration of 10 water molecules and an interlaminar distance of 11.5 Å. For this case, it is observed that equilibrium is reached after a few time steps, yielding an average interlaminar distance of 12.46 Å, an average water content of 27.6 molecules, and an average ethane content of 4.88 molecules per interlaminar space. It should be mentioned that other runs need a larger number of time steps for achieving equilibrium and so, runs must be monitored in order to establish the step range to average. In this case averages were performed in the range 5000-23000 steps. This same procedure was then repeated systematically for obtaining swelling curves for different reservoir and initial conditions.

Fig. 11 was built for ground level conditions and for a zero ethane partial pressure. It shows two swelling curves which differ on the initial conditions. One starts from an interlaminar distance of 11.5 Å and 10 randomly placed water molecules. The other one starts from an interlaminar distance of 16.0 Å and 60 water molecules. It can be seen that for $p/p_0 \leq 0.2$ both curves coincide, yielding interlaminar distances and water contents lower than 12.5 Å and 42 molecules, respectively. In particular, for $p/p_0 = 0$, no water molecules and 10.22 Å of interlam-

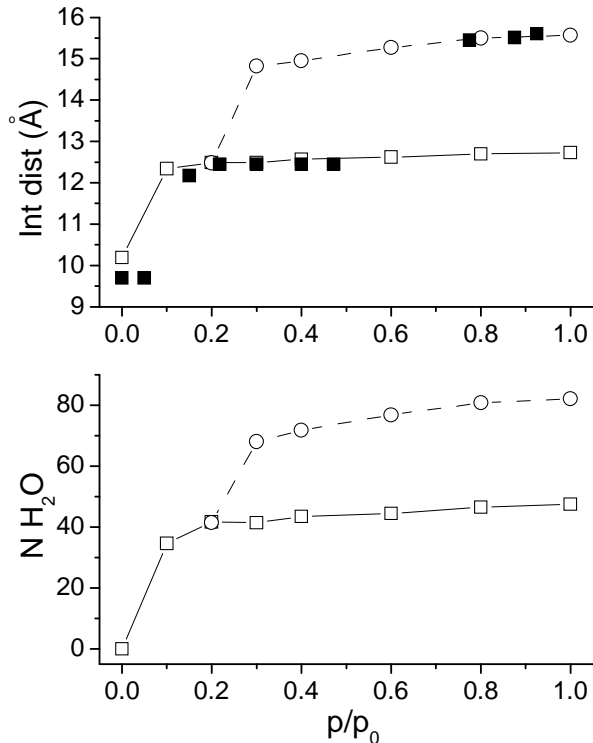


FIG. 11: Fig. 11: Interlaminar distance and number of water molecules per interlamina space as a function of water vapor pressure and for ground level conditions. The ethane partial pressure was set to zero. Symbols \square and \circ correspond to the data obtained by simulations and starting from 10 and 60 water molecules, respectively. Symbol \blacksquare corresponds to experimental data reported by Brindley and Brown [35].

interlaminar distance were obtained. For $p/p_0 \geq 2$, the curves separate producing two different plateaus. One corresponds to the formation of a single water layer and the other one to the formation of a double layer. This first plateau yields values of the interlaminar distance in the range 12.34-12.73 Å, having 34.6-47.5 molecules of water content. The double layer plateau yields 14.82-15.57 Å and 68.0-82.1 molecules, respectively. The interlaminar distance values are in good agreement with others reported by experiments and simulations [21, 24, 34, 35]. The water contents agree with the ones reported for the TIP4P water model and obtained by μVT simulations [24]. Nevertheless, they are larger than others [34].

The presented swelling curves are similar to those reported by Hensen and Smit [34]. Both predict a single layer for $p/p_0 \leq 0.2$ and two layers for the range $p/p_0 = 0.3-0.55$. For larger p/p_0 , our data still predict the two configurations to be stable and theirs show that the single layer is not stable anymore. This may be the main difference between both results. On the other hand, for a similar water-clay model and sampling from a μVT ensemble, Chávez-Páez *et al.* [24] also found that both configurations are stable, in good agreement with our data. Finally, swelling experimental data taken from Brindley

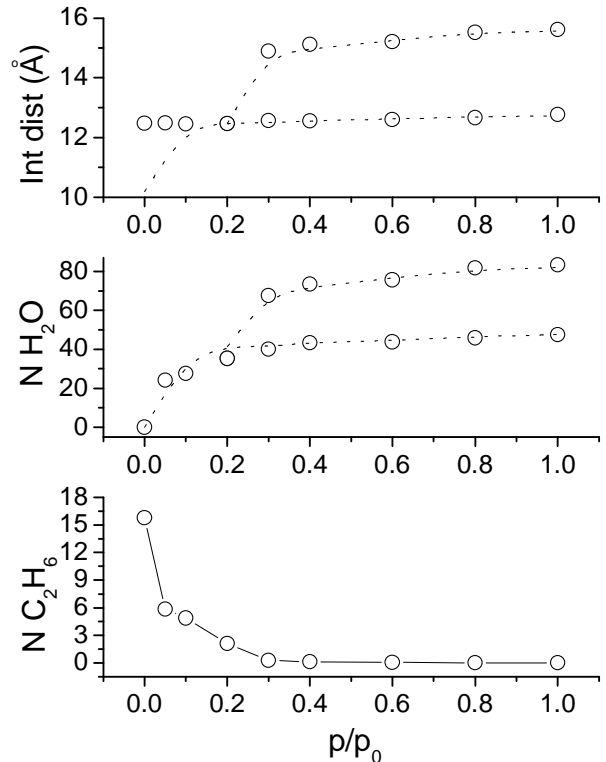


FIG. 12: Interlaminar distance, number of water molecules, and number of ethane molecules per interlamina space as a function of water vapor pressure. The ethane partial pressure, p_e , was set to 0.893P and ground level conditions were established. Dotted lines correspond to $p_e = 0$, which were included to make easy the comparison.

and Brown's work [35] were also included in the interlaminar distance graph, in order to be compared with our results. As can be seen, the agreement is very good.

A similar study was made to determine the influence of an ethane rich reservoir on the interlaminar space. For this purpose, a partial ethane pressure of 0.893P was set for the same ground level conditions. The obtained results are shown in Fig. 12 together with the curves already shown in Fig. 11. It is seen that, in general, they are very similar, *i. e.* there is not a very pronounced interaction between the ethane atmosphere in contact with the clay-water system. In fact, for $p/p_0 \geq 0.4$ the largest ethane content observed was 0.12 molecules per interlaminar space. This is equivalent to just one ethane per 350 water molecules. Furthermore, for the double-layer cases the ethane content is even lower, and this is why we did not include it in the plot. Moreover, the ethane proportion decreases with increasing the vapor pressure yielding zero for $p/p_0 \geq 0.8$. Consequently, those points obtained for $p/p_0 \geq 0.4$ practically show the same interlaminar distance and water content previously found.

Nevertheless, for $p/p_0 < 0.4$ a clear contribution of ethane to the interlaminar space can be seen. This contribution turns more important by decreasing the vapor

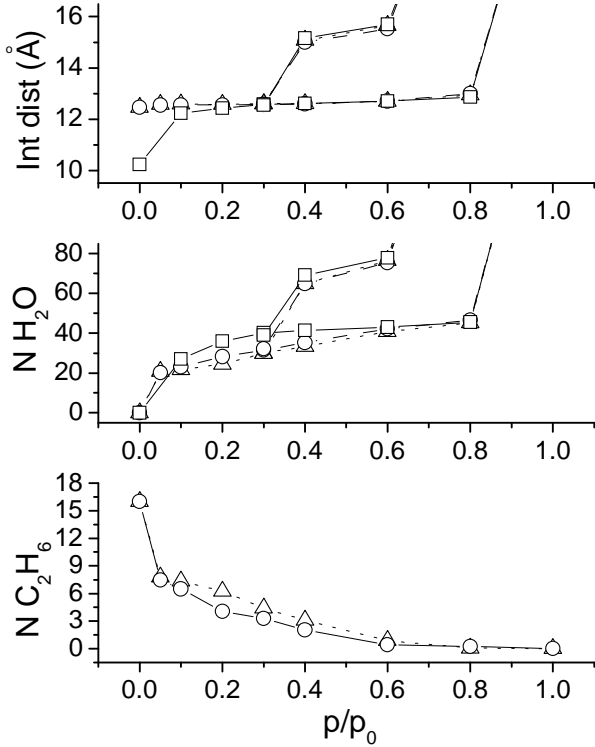


FIG. 13: Interlamellar distance, number of water molecules, and number of ethane molecules per interlamellar space as a function of water vapor pressure and for 4 km of burial depth. Symbols \square , \circ and \triangle correspond to $p_e=0.0\text{P}$, 0.107P and 0.268P , respectively.

pressure. This means that some water molecules are being replaced by ethane molecules, keeping the interlamellar distance almost constant. The exchange ratio is close to 3:1, as found in the preceding section. For the extreme case of $p/p_0=0$, the whole water layer is replaced by a layer of 16 nearly parallel ethane molecules, which leads to a practically equal interlamellar distance. It should be mentioned that, for this particular case, the simulation was started from 12.5 \AA of interlamellar space and 10 ethane molecules, instead of 11.5 \AA and 10 water molecules. If started from this last initial condition, the system quickly loses its water content producing a stable dehydrated state having zero ethane molecules. We also observed that this stable dehydrated state is destabilized by any small but enough vapor pressure. This indicates that the presence of a small amount of water, which widens the interlamellar space and solvate ions, aids the entrance of ethane molecules. This finding agrees with experimental evidence reported by Barrer [38].

Similarly to Fig. 12, Fig. 13 shows swelling curves but for 4 km of burial depth. Here, three different ethane partial pressures were considered. These are $p_e=0.0\text{P}$, 0.107P and 0.268P . For $p_e=0$, some differences with respect to the ground level case can be observed.

On the one hand, for $p/p_0=1.0$ neither a single layer

nor a double layer configuration are stable. For this particular case, no matter what the established initial conditions, the interlamellar space and water content monotonously increase as the simulation evolves. They were ended after reaching 180 water molecules and, therefore, we assume that a full hydration of the clay system was obtained. A similar behavior was observed for $p/p_0=0.8$ and for an initial configuration of 60 water molecules. When starting this last system from an initial configuration of 10 water molecules, however, the system reaches equilibrium yielding a single water layer. This is in good agreement with the results reported by Chávez-Páez *et al.* [14], where just a stable crowded single water layer configuration was obtained for burial conditions. Nevertheless, they obtain this behavior for $p/p_0=1.0$, instead of $p/p_0=0.8$. Their employed conditions were 353 K and 625 bar, which correspond to depths of 4.16 and 2 km, in terms of lithostatic and thermal gradients, respectively. Hence, it seems that the difference of temperature employed in both cases may explain the different values of p/p_0 that produces a stable single layer and an unstable double layer.

On the other hand, it is observed that both curves predict the same single water layer for $p/p_0 \leq 0.3$. Consequently, the double layer configuration is stable just in the range $p/p_0 = 0.4-0.6$. This result agrees with the experimental finding of a dehydration of the interlamellar space from a double water layer to a single one as the burial depth increases [36]. In addition, it also agrees with previous simulations of a similar system but for the MCY water model, where the stability of the two layer configuration was found to decrease with increasing burial depth [15].

Additionally, the interlamellar distances for single and double layer configurations are similar to those corresponding to ground level conditions. The water content, however, is slightly lower, suggesting that water molecules occupy a larger effective volume. This finding also agrees with the results reported for the MCY water model [15].

For $p_e=0.107\text{P}$ and 0.268P , a similar effect to the one found for ground level conditions is seen. That is, some water molecules are replaced by ethane molecules, and this exchange is enhanced for lower water vapor pressures. The extent of this exchange, however, is much larger under burial conditions. This is mainly explained by the higher ethane pressure, which leads to a larger ethane activity. Naturally, the water-ethane exchange is larger for $p_e=0.268\text{P}$ than for 0.107P for all cases, as expected. It is observed that even for $p/p_0=0.6, 0.4$ and 0.9 ethane molecules enter the interlamellar space for the single layer case and for $p_e=0.107\text{P}$ and 0.268P , respectively. This is approximately equivalent to one ethane molecule per 100 and 45 water molecules. For the double layer cases, the water-ethane exchange is not so pronounced. For $p_e=0.268\text{P}$ and $p/p_0=0.6$, only one ethane molecule per 220 water molecules were detected by averaging a large number of $\mu P_{zz}T$ ensemble configurations.

In spite of the important exchange of water by ethane molecules found for $p/p_0 \leq 0.6$, several water molecules still remain in the system even for p/p_0 as low as 0.05. For this case and for $p_e = 0.268P$, an average of 20.8 water molecules were found to be strongly attached to cations, impeding the entrance of more than 7.8 ethane molecules. As for the ground level case, when setting $p/p_0 = 0$, water is forced to leave the system and a single layer of 16 ethane molecules is obtained. Again, this layer is not obtained if the simulation is started from an initial configuration close to the dehydrated state. This means that a dehydrated clay containing just ions in its interlayer space and in contact with a dry ethane rich reservoir does not allow the entrance of ethane molecules.

IV. CONCLUSIONS

Hybrid Monte Carlo simulations in the $NP_{zz}T$ and $\mu P_{zz}T$ ensembles were used for studying the Namontmorillonite hydrates under ethane rich reservoirs. From the $NP_{zz}T$ study, interlaminar distances as a function of the water and ethane content were obtained. These curves show clear plateaus for lower ethane contents and mainly for water contents consistent with the formation of a single water layer.

On the other hand, from the $NP_{zz}T$ ensemble we also studied the interlayer structure. Here it was observed, for systems containing few ethane molecules and water enough to complete a single layer, that ethane mainly situates close to the interlayer midplane and adopts a

nearly parallel arrangement to the clay surface. Furthermore, it was observed that the water-ion-clay interactions are practically unchanged by the presence of the hydrocarbon, indicating that this component is being left aside.

In addition, the $\mu P_{zz}T$ ensemble allows us determining the interlaminar distance and water-ethane content for any specific reservoir's conditions. Hence, several swelling curves as a function of water pressure were obtained. For ground level conditions, they indicate that ethane molecules do not practically enter the interlaminar space, unless one establishes a very low water pressure. If this is the case, we also observed that water molecules are flushed out by this entrance, leading to an almost constant interlaminar space close to 12.5 Å.

For the studied burial depth conditions, it was observed that the exchange is enhanced, and that the ethane molecules are capable of entering even for relatively large water pressures. On the other hand, this exchange is not very pronounced for a double layer configuration. Furthermore, it was observed that for very low water pressures, the system holds water enough to keep the ions' shells practically intact. Finally, our results also indicate that a dehydrated and collapsed clay system is not capable to swell and absorb ethane molecules if no water vapor is present in the atmosphere.

V. ACKNOWLEDGMENTS

This research was supported by Instituto Mexicano del Petróleo grant No D.00072. The authors would like to thank Dr. L. de Pablo for his useful comments.

-
- [1] A. C. D. Newman, *Chemistry of Clays and Clay Minerals* (Mineralogical Society, London, 1987).
 - [2] F. K. North, *Petroleum Geology* (Unwin Hyman, Boston, 1990).
 - [3] F. Chou Chang, N. T. Skipper, and G. Sposito, *Langmuir* **11**, 2734 (1995).
 - [4] F. Chou Chang, N. T. Skipper, and G. Sposito, *Langmuir* **14**, 1201 (1998).
 - [5] M. Chávez-Páez, L. de Pablo, and J. J. de Pablo, *J. Chem. Phys.* **114**, 10948 (2001).
 - [6] S. Park and G. Sposito, *J. Phys. Chem. B* **104**, 4642 (2000).
 - [7] E. S. Boek, P. V. Coveney, and N. T. Skipper, *J. Am. Chem. Soc.* **117**, 12608 (1995).
 - [8] E. S. Boek and M. Sprik, *J. Phys. Chem. B* **107**, 3251 (2003).
 - [9] F. Chou Chang, N. T. Skipper, and G. Sposito, *Langmuir* **13**, 2074 (1997).
 - [10] R. Sutton and G. Sposito, *J. Colloid Interface Sci.* **237**, 174 (2001).
 - [11] V. Marry and P. Turq, *J. Phys. Chem. B* **107**, 1832 (2002).
 - [12] D. A. Young and D. E. Smith, *J. Phys. Chem. B* **104**, 9163 (2000).
 - [13] A. V. C. De Siqueira, N. T. Skipper, P. V. Coveney, and E. S. Boek, *Mol. Phys.* **92**, 1 (1997).
 - [14] L. de Pablo, M. L. Chávez, A. K. Sum, and J. J. de Pablo, *J. Chem. Phys.* **120**, 939 (2004).
 - [15] G. Odriozola and F. Guevara, *Langmuir* **20**, 2010 (2004).
 - [16] S. H. Park and G. Sposito, *J. Phys. Chem. B* **107**, 2281 (2003).
 - [17] J. O. Titiloye and N. T. Skipper, *Chem. Phys. Lett.* **329**, 23 (2000).
 - [18] B. J. Teppen *et al.*, *J. Phys. Chem. B* **101**, 1579 (1997).
 - [19] G. Sposito *et al.*, *Proc. Natl. Acad. Sci.* **96**, 3358 (1999).
 - [20] W. L. Jorgensen, J. Chandrasekhar, and J. D. Madura, *J. Chem. Phys.* **79**, 926 (1983).
 - [21] E. S. Boek, P. V. Coveney, and N. T. Skipper, *Langmuir* **11**, 4629 (1995).
 - [22] S. K. Nath, F. A. Escobedo, and J. J. de Pablo, *J. Chem. Phys.* **108**, 9905 (1998).
 - [23] N. T. Skipper, F. Chou Chang, and G. Sposito, *Clays Clay Miner.* **43**, 285 (1995).
 - [24] M. Chávez-Páez, K. Van Workum, L. de Pablo, and J. J. de Pablo, *J. Chem. Phys.* **114**, 1405 (2001).
 - [25] S. K. Nath, F. A. Escobedo, and J. J. de Pablo, *J. Chem. Phys.* **108**, 9905 (1998).
 - [26] D. G. Bounds, *Mol. Phys.* **54**, 1335 (1985).
 - [27] V. Marry, P. Turq, T. Cartailleur, and D. Levesque, *J. Chem. Phys.* **117**, 3454 (2002).

- [28] J. Alejandro, D. J. Tildesley, and G. A. Chapela, *J. Chem. Phys.* **102**, 4574 (1994).
- [29] M. P. Allen and D. J. Tildesley, *Computer Simulation of Liquids* (Clarendon, Oxford, 1986).
- [30] B. Mehlig, D. W. Heermann, and B. M. Forrest, *Phys. Rev. B.* **45**, 679 (1992).
- [31] M. Tuckerman and B. J. Berne, *J. Chem. Phys.* **97**, 1990 (1992).
- [32] E. J. M. Hensen, T. J. Tambach, A. Blik, and B. Smit, *J. Chem. Phys.* **115**, 3322 (2001).
- [33] D. Frenkel and B. Smit, *Understanding molecular simulation* (Academic, New York, 1996).
- [34] E. J. M. Hensen and B. Smit, *J. Phys. Chem. B* **106**, 12664 (2002).
- [35] G. W. Brindley and G. Brown, *Crystal Structures of Clay Minerals and their X-Ray Identification*, 5 ed. (Mineralogical Society, London, 1984).
- [36] N. T. Skipper, G. D. Williams, A. V. C. de Siqueira, and C. Lobban, *Clay Minerals* **35**, 283 (2000).
- [37] F. Din, *Thermodynamic functions of gases* (Butterworths, London, 1961).
- [38] R. M. Barrer, *Zeolite and Clay Minerals as Sorbents and Molecular Sieves* (Academic Press, London, 1978).